Optimization of spot pattern in indoor diffused optical wireless systems

by

Madhusudhana Reddy Lebaka

DEPARTMENT OF ELECTRICAL ENGINEERING

INDIAN INSTITUTE OF TECHNOLOGY, KANPUR

June 2006

Optimization of spot pattern in indoor diffused optical wireless systems

A Thesis Submitted

in Partial Fulfillment of the Requirements

for the Degree of

Master of Technology

by

Madhusudhana Reddy Lebaka

to the

DEPARTMENT OF ELECTRICAL ENGINEERING

INDIAN INSTITUTE OF TECHNOLOGY, KANPUR

June 2006

CERTIFICATE

It is certified that the work contained in the thesis entitled "*Optimization of spot pattern in indoor diffused optical wireless systems*" by *Madhusudhana Reddy Lebaka* has been carried out under my supervision and that this work has not been submitted elsewhere for a degree.

(Dr. Y.N.Singh)

June 2006

Associate Professor,
Department of Electrical Engineering,
Indian Institute of Technology,
Kanpur-208016.

ACKNOWLEGGEMENTS

I would like to express my gratitude to my advisor, Dr. Y. N. Singh, for his both insight and broad range of knowledge that he willingly shared with me during the research and writing of my dissertation. His advices are always very helpful, both academically and non-academically. It has been a great pleasure working with him. I also would like to extend my sincere thanks to Mr. A. Sivabalan, for his encouragement, help and support.

I express my appreciation and indebtedness to my friends G. Praveen, D.Sreenivas, P. Pathak, V. Srinivas, Anarul Islam, Rajat, and Rajeev who helped me in many ways during my thesis work.

Madhusudhana Reddy Lebaka

DEDICATED

to

MY PARENTS and SISTER

ABSTRACT

Simulated Annealing(SA) algorithm is proposed to be used in the optimization of the spot pattern for the indoor diffuse optical wireless systems.The channel Response is analyzed using conventional grid-based patterns and a field of view (FOV) of 30° is found to give a good performance balance in the uniformity of the received power distribution and multipath dispersion. Using the algorithm, the optimized spot pattern is found for minimizing the ratio of standard deviation of the received power to the average received power level. It resulted in more than 50% improvement.

Contents

List of Figures

List of Tables

GLOSSARY

APD	Avalanche Photo Diode
BER	Bit Error Rate
CGH	Computer Generated Hologram
DD	Direct Detection
FOV	Field of View
IM	Intensity Modulation
IrDA	Infrared Data Association
LAN	Local Area Network
LD	Laser Diode
LED	Light Emitting Diode
LOS	Line Of Sight
MAC	Medium Access Control sub-Layer
OOK	On Off Keying
OSI	Open Systems Interconnection
PIN	P Intrinsic N
PPM	Pulse Position Modulation
RZ	Return to Zero
SA	Simulated Annealing

Chapter 1

INTRODUCTION

The emergence of portable computing devices such as laptops, palmtops and personal digital assistants has fulled the demand for mobile connectivity and hence, led the development of wireless local area networks(LANs). Wireless communications have always offered an alternate solution to the fixed network, which introduce difficulties in construction and rewiring during the initial system setup and later during the expansion phases. The benefits of an alternative flexible network are many in terms mobility and portability. Trends in communication suggest that the future network consist of fiber-optic network and wide band wireless short-range access over a wireless channel. Portable terminals should have access to all of the services that are available on high-speed networks. Unlike their wide counterparts, portable devices are subject to severe limitations on power consumption,size and weight. The desire for inexpensive, high-speed links satisfying these requirements has motivated the recent interest in infrared wireless communication.

Traditionally, radio frequency transmission was used in wireless applications. However, the RF spectrum is so congested that it is very difficult to accommodate high bit rate applications. The optical systems with low implementation complexity and no spectrum license requirements provide a possible solution. The optical infrared energy can typically confine within the communication environment. This eliminates the problems of interference generated by neighboring users and offers a degree of security at the physical layer level. The

transmission equipment and optical wavelength can be reused at other parts of the building. Optical wireless systems also offer immunity from signal fading, which is a major problem in RF communication systems. As such, indoor infrared communications has recently gained importance, especially in view of the increased data mobility requirements of users for both computing and communications.

Infrared communications were mainly studied during 1960's as an alternative for mobile radio communications. But, no real system for indoor coverage using infrared links was seriously considered. Recently, infrared has gained ground with operators seeking to cover area that require high bit rate services such as the office areas. Serious work on indoor optical wireless systems started during early 90's. At present it is a very rapidly developing research are and there is huge interest and commitment in this area by major communication industries due to its enormous commercial applications.

In order to correctly and reticently deploy a communication system, the system designer must have a sound knowledge of the channel. This can be done through experimentation and modeling with methods that are accurate enough for all significant channel characteristics.

This thesis deals mainly with the study of different spot patterns in indoor diffused optical wireless systems. Simulation studies are done on the various properties of the optical signal, and receiver. The main objectives of the work are discussed in the following section.

1.1 Thesis Objectives

The Objective of the thesis is to optimize the spot patterns so as to receive uniform power all through the receiving plane. *Multiple Bounce Impulse Response Model* and *Simulate annealing* algorithm are used for simulation. The objectives are summarized as follows.

- To find RMS delay spread of the transmitted optical signal due to multipath propagation.
- To study the effect of field of view (FOV) on the received signal.

- To study the effect of spot pattern on the received signal.
- To find the optimized spot pattern at various FOVs, for which, the received power is uniform through out the receiving plane.

1.2 Thesis Organization

Chapter 2 gives a review of the indoor optical wireless systems. The basic components of optical wireless systems and link configurations are discussed. A brief literature survey of infrared channel modeling and characterization is also presented. Chapter 3 summarizes theoretical background of the indoor channel characterization and simulation studies of channel. Chapter 4 deals with simulation studies of power distribution in the receiving plane for various spot patterns and optimization patterns. The results are also discussed. Chapter 5 presents the conclusions of the work and future improvements that may be possible.

Chapter 2

REVIEW OF INDOOR INFRARED WIRELESS SYSTEMS

2.1 Introduction

The wireless systems widely used today utilizes radio waves, but this alone may not be sufficient for the future. Modern digital communication systems require high data rate capabilities. However, the radio spectrum is regulated and saturated. An alternative medium is infrared communications, which appear to be very attractive way to complement radio.

Infrared communications have found many areas of use. Almost every home includes a television set which is controlled by an infrared remote control. Also, there is a standard for communication between two computers using infrared. This standard is called IrDA (Infrared Data Association), and has been included in almost every portable computer and mobile phone. This supports speed up to 115kb/s but the limiting factor is distance between the terminals should be low, and a line of sight (LOS) is always needed. Infrared communications are very successful in the field of directed communication between two buildings. although very high data rates up to hundreds of Mb/s can be achieved, it has disadvantage of being unsustainable in heavy weather conditions such as snowfall or fog. The link cannot be sustained then, due to the increased path loss between terminals.

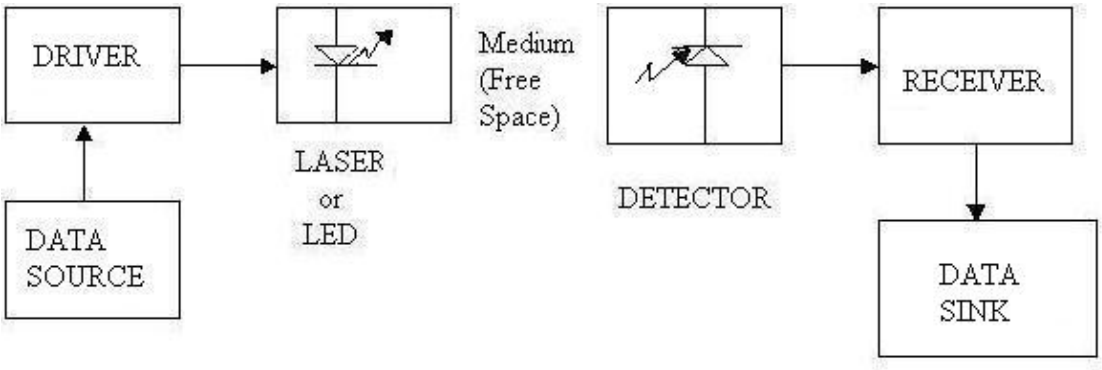

Figure 2.1: Block Diagram of an Optical wireless Communication link

This chapter presents a small review of the indoor infrared wireless communication system. It explains the basic components, link configurations, a comparison with radio, and literature survey of the important works in this field. finally, Some of the practical systems reported are discussed.

2.2 Basic Optical Wireless System

The basic sub system of an optical wireless system are *transmitter* based on either (LEDs or LDs), the *channel* (the medium between the transmitter and the receiver)and the *receiver* based on (PIN or APD based). The link length can vary from a few meters to a few km. The block diagram of a typical optical wireless communication link is shown in Fig.2.1.

The electrical information signal produced by the source modulates an optical carrier. The one commonly used is Intensity Modulation (IM). The modulated optical carrier is propagated through the channel. At the receiver, the received optical field is optically collected and converted back to an electrical signal by a detector, which is further processed by electronic stages to recover the original information with an acceptable level of error.

2.2.1 Transmitter

The transmitter side consists of the data source, driver circuits and the light source. There are two basic light sources, the LD and the LED. Since eye safety is a major consideration for indoor applications, the optical source need to be chosen carefully. LEDs are the preferred choice for indoor use. Since the light intensity of an LED may not be sufficient for most applications, LED arrays may have to be used. Another popular solution is to use a laser diode with a diffuser. A comparison between the characteristics of LEDs and the LDs [1] are given in table 2.1

Characteristics	Light Emitting Diodes	Laser Diodes
Spectral Width	25-100 nm	$< 10^{-5}$ to 5 nm
Modulation Bandwidth	Tens of KHz to tens of MHz	Tens of MHz to tens of GHz
E/O Conversion Efficiency	10 to 20%	30 to 70%
Eye Safety	Generally considered eye safe	Must be rendered eye-safe. Especially for $\lambda < 1400$nm
Cost	Low	Moderate to high

Table 2.1: Comparison between LEDs and LDs

2.2.2 Free Space Medium

The link budget for a free space link are strongly determined by the atmospheric loss along the propagation path, which comprises of free space loss, clear air absorption, scattering, refraction, and scintillation. All forms of optical wireless systems experience free space loss. Other sources of atmospheric losses are applicable to long distance systems only. Free space loss defines the portion of optical power arriving at the receiver that is usefully captured within the receiver's aperture.

2.2.3 Receiver

The function of the receiver is to convert optical signal back to the original electrical signal. Receiver consists of a PIN or APD photodetector, preamplifier receiver circuit. PIN or APD operate in reverse bias, also known as photoconductive mode of operation. The advantages of photoconductive operation are high speed, lower capacitance, and better linearity.

The photodetector and amplifier are sources of noise at the receiver side. The noise in a photodiode can be of two types; the first one is called the shot noise due to dark current and received optical signal. and the second one is called thermal noise due to shunt resistance, also known as Johnson noise. The important requirements on the photodiodes for optical wireless communication are high quantum efficiency, fast response time, low capacitance, low dark current, and low avalanche excess noise. It is desirable to use a large area photodetector since shot noise can be reduced, SNR is proportional to the detector area. However large area detectors have high capacitance, which can limit receiver bandwidth and greatly increase thermal noise. It is desirable to reduce the required detector physical area by the use of an optical concentrator, which accepts light from a large collection area and concentrates it to the smaller detector area.

2.3 Comparison between Radio and Infrared

Infrared communication offer advantages and some disadvantages when compared with the analogous radio links. Table 2.2 gives a comparison between the two systems [2].

As seen from the comparison, infrared shares some properties with radio, although there are some significant differences. These are discussed in detail below.

- Multipath fading is not present in infrared channels, since the area of the receiving photodetector spans several thousands of wavelengths. the output current of the photodiode will be proportional to the integral of the squared electric field over the entire area of photodiode surface. thus a single photodetector can provide a significant spatial diversity, which will prevent multipath fading. Multipath dispersion is present in

Property	Radio	Infrared
Path Loss	High	High
Multipath Fading	Yes	No
Multipath Dispersion	Yes	Yes
Bandwidth Limitation	Regulatory	Photodiode
Dominant Noise	Interference	Background Noise
Signal Transmitted	Amplitude	Power
Wall penetration	Yes	No

Table 2.2: Comparison between Infrared and Radio Channels

infrared channels also. If a short pulse is sent through the channel, the pulse broadens due to dispersion and inter symbol interference occurs. The dispersion is the result of the reflective properties of the channel, which transforms a narrow pulse into wider version. This limits the data rate and increases the bit error rate.

- In radio, the main limitation of bandwidth is due to regulation, since the bandwidth has to be licensed before being used. In infrared limitation is posed by the channel and various devices.

- The dominant noise in cellular communications is interference from adjacent cells. In infrared systems, noise comes from the background. The three main sources of ambient light are sunlight, incandescent lamps and fluorescent lamps [3],[4],[5]. Infrared links cannot sustain operations in direct sunlight, unless spatial filters or very directional sources and receivers are used. Artificial sources of ambient light produce a periodic interference signal in infrared wireless receivers which, if ignored, has the potential to degrade link performance. These lights have a wide spectrum and they also emit higher power infrared radiation during warm up thus degrading infrared communication.

- Although the infrared channel is related to the linear gaussian channel, there is a difference between the two. The input of infrared channel represents power and not

amplitude unlike radio. This gives raise to two constraints; first, the signal must be positive and its average value must not exceed a prescribed value[6] for safety reasons.

The transmitted power in the infrared domain is described by

$$\lim_{T\to\infty} \frac{1}{2T} \oint_{-T}^{T} x(t)dt \leq P \tag{2.1}$$

where

- x(t) is the instantaneous value of the transmitter signal(Watts).
- P is the maximum value of the power allotted to be transmitted due to safety reasons.
- T is the duration of communication(sec).

- Infrared radiation does not penetrate opaque objects, and walls efficiently separate two cells. Security is high since the radiation is confined within the cell. On the other hand, less coverage can be achieved with an infrared link, and base stations have to be placed within every room of operation.

The following points summarize the advantages and drawbacks of infrared communications over radio.

- Infrared offers unregulated bandwidth: 200Thz in the 700-1500nm range.
- There is no interference from adjacent cells and security is very high,
- No multipath fading.
- Higher capacity per unit volume.
- Cost effective at rates above 100 Mb/s.

The draw backs are

- Multipath dispersion is present.

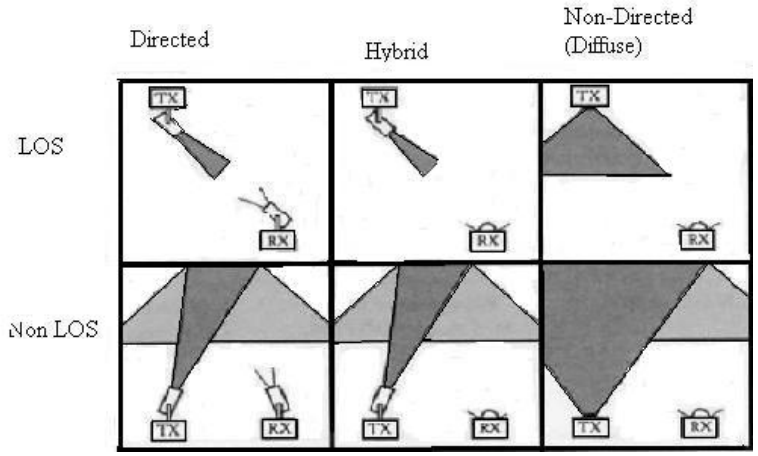

Figure 2.2: Classification of Infrared Links

- Large amount of radiations can be harmful to humans.
- Strong interference from daylight, light sources, remote controls and other devices.

2.3.1 Link Configuration

Indoor optical wireless can employ various designs, and it is convenient to classify them according to two criteria.This classification scheme is shown in Fig.2.2[1].

The first section is directionality of the transmitter and receiver. Directed links employ directional transmitters and receivers, which must be aimed in order to establish a link. Non directed links employ wide-angle transmitters and receivers, alleviating the need for pointing. Directed link design maximizes power efficiency, since it minimizes path loss and reception of ambient noise. On the other hand, non directed links may be more convenient to use, particularly for mobile terminals, since they do not require aiming to the transmitter or receiver. It is also possible to establish hybrid links, which combine transmitters and receivers having different degrees of directionality.

The second classification criterion to whether the link relies upon the existence of an uninterrupted LOS path between the transmitter and receiver. LOS links rely upon such a path, while non-LOS relies upon reflection of the light from the ceiling or some other diffusely

reflecting surface. LOS link design maximizes power efficiently and minimizes multipath distortion. Non-LOS link design increases link robustness and ease of use, allowing the link to operate even when barriers are there between the transmitter and receiver. The greatest robustness and ease of use is achieved by the non directed-non-LOS link design which is often referred to as diffuse link.

2.3.2 Line of Sight Systems

Line of Sight systems employ high degree of directionality of the transmitter and receiver and uninterrupted LOS. LOS link design maximizes power efficiency and minimizes multipath distortion. The performance of the link relies up on the existence of an uninterrupted LOS path between the transmitter and receiver. The main drawback is the lack of mobility and susceptibility to blocking. The optical sources must be Class 1 eye safe; hence LEDs have to be used in place of LDs which limits the capacity to few megabits per second.

These types of links are used for applications in which the terminals are relatively fixed, such as desktop computers in office. One of the most widely adopted standards is the IrDA.

2.3.3 Diffuse Systems

The greatest robustness and ease of use is achieved by the non-directed, non-LOS design, which is often referred to as diffuse link. However, diffuse systems have a higher path loss than their LOS counter parts, requiring higher transmitter power and a receiver having large light collection area.

This type of topology overcomes the blocking problem by relying on the high reflectivity of common building materials, so that a significant fraction of the received signal arrives at the receiver from a number of angles. Such as topology is extremely flexible and can be used in either organized or ad-hoc networks. However the bit rate that can be achieved is very less compared to the LOS systems. In addition, optical losses associated with the link are much greater than LOS systems.

In case of an entirely diffuse link, the optical power launched into a closed room is scattered by the walls, ceiling, floor and furniture. After some reflections the irradiance is almost uniform, so that detector need not be oriented towards the transmitter. Full mobility within the room is allowed and there is no shadowing effects caused by moving persons or machines. There are two limitations for diffuse links: The optical power has to be large enough to cover the whole volume, and multipath dispersion limits the data rate. Multipath propagation causes the a spread of transmitted pulse, which may result in loss of pulse amplitude and inter symbol interference. Hence, there is a maximum transmission speed which depends on the room size and reflection coefficients inside the room.

2.4 Current Infrared Communication System

At present, most infrared links are of the directed-LOS or hybrid-LOS designs. The low path loss of these designs minimizes the transmitter power requirement and permits the use of a simple, low-cost receiver. Typically, these links transmit using a single LED, which emits an average power of several tens of mW that is concentrated within a semiangle of 15° to 30°. The LED emission wavelength typically lies between 850 and 950 nm. This wavelength matches the responsivity peak of the silicon p-i-n photodiode. In hybrid-LOS link designs, the photodiode is most often encapsulated in a planocylindrical or hemispherical plastic lens that serves to concentrate the received light, while maintaining a relatively wide FOV, e.g., a semiangle of the order of 60°. Directed-LOS links employ an optical concentrator that restricts the FOV, usually with the goal of providing a higher degree of optical concentration. Directed-LOS and hybrid-LOS links are relatively free from multipath distortion, sometimes permitting them to achieve bit rates above 100 Mb/s while maintaining a very simple design. These link designs are well-suited for point-to-point and some point-to-multipoint applications, but are not suited for multiple-access networks, since it is difficult to establish full bidirectional connectivity between more than two transceivers. Directed-LOS and hybrid-LOS links have been used for many years in remote-control units and other

unidirectional, low-bit-rate applications.

2.5 The IrDA Standard for Very Short Distance Point-to-Point Systems

Over the past seven years, the IrDA has established standards for short-range, half-duplex LOS links operating at bit rates up to 4 Mb/s [12]. Two of the key features of IrDA transceivers are low cost and low power consumption (under 1 W while transmitting, and under 100 mW when idle or receiving). At present, more than 160 companies worldwide are members of IrDA.

There are several key components of the IrDA standards [12]. The IrDA Serial Infrared Physical Layer defines standards for half-duplex links at several bit rates up to 4 Mb/s. 4 Mb/s links employ 4-pulse-position modulation (4-PPM), while 1.152 Mb/s links utilize on-off keying (OOK) with return-to-zero (RZ) pulses having a duty cycle of 0.25. Links operating at bit rates of 115.2 kb/s and below employ OOK with RZ pulses having a duty cycle of 0.1875 (shorter pulses are permitted in some cases). IrDA-compliant transmitters must emit at a wavelength between 850 and 900 nm into a semiangle (at half-power) of 15° to 30°. Compliant receivers must have a FOV (semiangle at half-effective light-collection area) of at least 15°. Most IrDA receivers have a much larger FOV, so that most IrDA links are of the hybrid-LOS type. IrDA links are required to achieve a bit-error rate (BER) not exceeding 10^{-9} (10^{-8} for 4 Mb/s links) over a range of at least 1 m, but many links achieve a range as long as 3 m.

2.6 Other Standards used in Diffused Infrared Systems

The main importance of standards is to provide wireless connectivity to automate machinery, equipment or stations that require rapid deployment, which may be portable or hand held or which may be mounted on moving vehicles with local area. The other importance is to

offer a standard for use by regulating bodies to standardize access to one or more frequency bands for the purpose of local communication.

2.6.1 Different IEEE 802 Standards

The IEEE has produced several standards for Local Area Networks. These standards, collectively known as IEEE 802, include CSMA/CD, CSMA/CA, Token bus, Token ring, etc. The various standards differ at the physical layer and Medium Access Control (MAC) sublayer, but are compatible at the data link layer. The IEEE 802 standards have been adopted by American National Standard (ANSI), by NIST as government standards, and by ISO as international standards (known as ISO-8802). IEEE 802.11 standard describes Diffused IR & RF Wireless Local Area Network.

2.6.2 Scope of Effort of IEEE 802.11 Standard

The scope of effort of IEEE 802.11 standard is to define physical layer wireless data networking and physical layer transmissions (PHY) by radio or infrared and Medium Access Control (MAC) Protocol compatible with the existing standards for higher layers. The IEEE standard for wireless LAN started in 1988 as IEEE 802.4L as a part of the IEEE 802.4 Token bus wired LAN standard.

In 1990, the IEEE 802.4L changed its name to IEEE 802.11 to form a stand alone Wireless LAN standard in the IEEE 802 LAN standard organization and several draft standards have been published for review. With long effort, the IEEE 802.11 group developed framework to incorporate wireless specific issues such as power control, frequency management, roaming and PHY and MAC Protocol sub-layer in LAN standards.

The IEEE 802.11 draft standard describes mandatory support for 1 Mb/s Wireless LAN with optional support for a 2 Mb/s data transmission rate. at present there are two emerging LAN standards in use, as mentioned below.

1. European Telecommunication standards institute's High Performance European Radio

LAN (HIPERLAN), for data rates upto 23.529 Mb/s.

2. The IEEE 802.11 standard for Wireless LAN.

Both draft standards cover the PHY and MAC sub-layer of the open systems interconnection (OSI) seven layer reference model.

Through judicious use of the technologies employed in currently available systems, it is possible to enhance the performance of wireless infrared systems significantly. It appears likely that 10-Mb/s diffuse links and low-cost LOS links operating at tens of Mb/s can be achieved. Even higher bit rates will be desirable in future applications. Recent research work suggests that using new techniques, low-cost infrared links operating in the 100 Mb/s range may be achieved.

Chapter 3

INFRARED CHANNEL MODELING

This chapter describes the tools used to model the infrared channel. The channel under study is the infrared diffuse channel, in which there is no need for LOS between the transmitter and receiver. Communication may rely on scattered radiation from the walls of the room. In this way, mobility is increased, and shadowing does not have a large impact on the link.

3.1 Multi-Receiver Channel Estimation

In this discussion we limit considerations to rectangular rooms, although techniques can be easily extended to other geometries. Next we define the models for the source, reflectors, and receiver.

3.1.1 Site and Link Model

We model optical wireless channels formed by a transmitter and receiver placed inside a reflective environment, as depicted in Fig. 3.1(b). The transmitter or source S_j is a LD or a LED transmitting a signal $X_j(t)$ using IM. We first consider a collection of receivers, each with a photodiode with responsivity r and using DD. These receivers may be either a group

of receivers being used as an angle-diversity receiver, as in [13], or they might represent a collection of alternative single receiver locations that are being considered together. We will show that considering all receiver locations and orientations concurrently will bring substantial savings in channel estimation computation time.

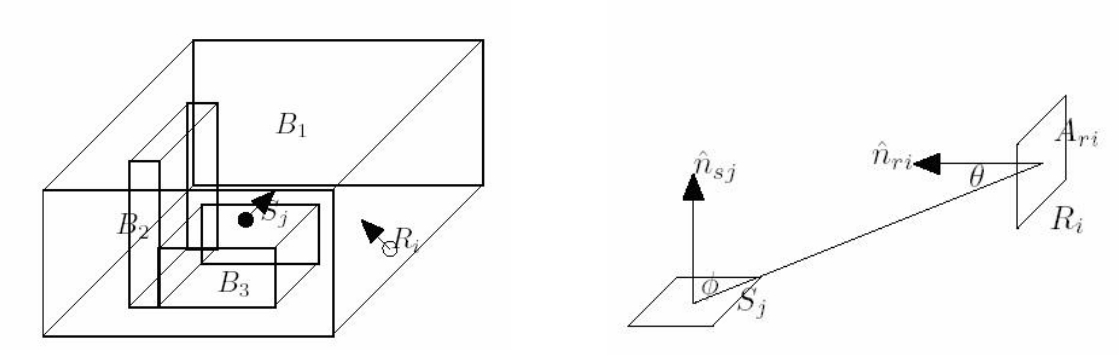

(a) Environment

(b) Source and Receiver

Figure 3.1: Site and Link Model

3.1.2 Channel Model

When source S_j is transmitting receiver R_i is receiving, the current from the photodiode is

$$Y_{ij}(t) = rX_j(t) * h_{ij}(t) + N_j(t), \tag{3.1}$$

where $*$ denotes convolution, $h_{ij}(t)$ the impulse response of the channel between source S_j and receiver R_i, and $N_i(t)$ the noise at the receiver. The baseband impulse response $h_{ij}(t)$ for IM/DD communication [14] is completely determined properties of source S_j, receivers R_i, and environment E. Hence, we will write $h_{ij}(t)$ more specifically as $h_E(t; S_j, R_i)$. Although we consider multiple transmitters and receivers, here its been restricted to [1] a single transmitter and a single receiver at a time. If multielement transmitters are employed, then the signal

received by receiver $R_i$would be

$$Y_{ij}(t) = \sum_{j=1}^{J}(rX_j(t) * h_{ij}(t)) + N_j(t), \tag{3.2}$$

where the transmitted signals $X_j(t)$ might be carrying the same or different information sequences. A multielement receiver employing combining would receive the signal

$$Y_i(t) = \sum_{i=1}^{I}(\alpha_i Y_{ij}(t - \tau_i)). \tag{3.3}$$

3.1.3 Source and Receiver

The source S_j is described by a position vector $\overrightarrow{r}_{sj}$, an orientation vector $\widehat{n}_{sj}$ and a radiant intensity pattern $T(\phi)$, where we assume for simplicity that the radiant intensity pattern has axial symmetry about the normal. A typical model for radiant intensity pattern is the Lambertian of order n given by

$$T(\phi) = \frac{n+1}{2\Pi}\cos^n(\phi). \tag{3.4}$$

The receiver R_i is described by a position vector $\overrightarrow{r}_{ri}$, an orientation vector $\widehat{n}_{ri}$, an optical collection area A_{ri}, and an effective area at incident angles θ of $A_i(\theta) = A_{ri}g_i(\theta)$ is again modeled as axial symmetric. This allows for a very general description of the receiver optical system. A typical model for a bare photodiode is that $g(\theta) = \cos(\theta)$; the cosine dependence models the decline in effective area for light incident on planar detectors at non-normal incidence.

3.1.4 Environment

The environment E is modeled as a set of N_b rectangular boxes $\{B_1, ..., B_{Nb}\}$, as depicted in Fig.3.1(a). The first box B_1 represents the universe in which all other boxes and all sources and receivers are contained. This can represent a single room, a floor, or even an entire building. Interior objects are described by single boxes or combinations of boxes. This method allows for inclusion of such objects as wall partitions, doorways, desks, chairs, and

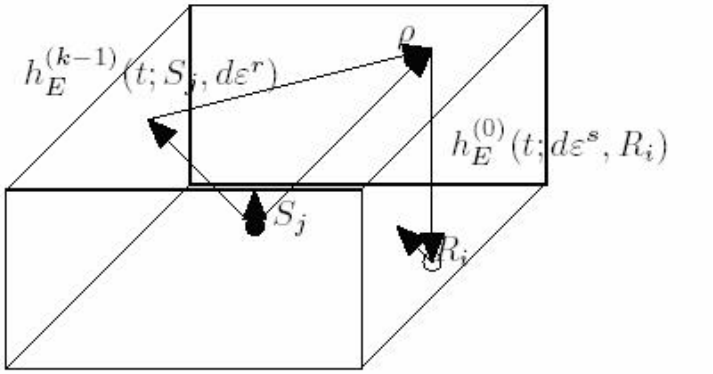

Figure 3.2: Impulse Response Calculation

people. The boxes are further modeled as having six opaque internal faces and six opaque external faces. Only the exterior faces of the internal boxes $\{B_2, ..., B_{Nb}\}$ are relevant, and only the internal faces of the universe box B_1 are relevant, for a total of $6N_b$ reflecting faces. Each face F_i is modeled as a diffuse reflective surface (Lambertian) of reflectivity ρ_{Fi} The receivers and transmitters are not included as boxes, so their packaging must be explicitly included if it is significant to the problem at hand.

3.2 Impulse Response Calculation

Impulse response calculation follows the basic methodology outlined in [15] with extensions for arbitrary transmitter and receiver gains and multiple transmitters and receivers. The calculation involves decomposition into bounces, discretization into facets, and finally multi-receiver iteration. We then present an equivalent formulation for a multi-transmitter calculation.

3.2.1 Decomposition into Bounces

All transmitted light arriving at the receiver has undergone a definite number of reflections or bounces. Hence, we can decompose the impulse response $h_E(t; S_j, R_i)$ as

$$h_E(t; S_j, R_i) = \sum_{k=0}^{\infty} h_E^k(t; S_j, R_i), \tag{3.5}$$

where $h_E^k(t; S_j, R_i)$ is the impulse response due to signal light undergoing exactly k bounces during its path from the source S_j to the receiver R_i.

The line of sight impulse response $h_E^0(t; S_j, R_i)$ is given by

$$h_E^0(t; S_j, R_i) = V(\overrightarrow{r}_{sj}, \overrightarrow{r}_{ri}, E)T(\Phi_{ij})(A_{ri}g(\theta_{ij})/D_{ij}^2)\delta(t - D_{ij}/c), \tag{3.6}$$

where $D_{ij} = |(\overrightarrow{r}_{sj} - \overrightarrow{r}_{ri})|$ is the distance between the source and receiver. The visibility function $V(\overrightarrow{r}_{sj}, \overrightarrow{r}_{ri}, E)$ is 1 when the LOS path between S_j and R_i is unobstructed, and is zero otherwise.

Now, the K-bounce response can be calculated using the (K-1)- bounce response using

$$h_E^k(t; S_j, R_i) = \int_E \rho_{d\epsilon^r} \cdot h_E^{k-1}(t; S_j, d\epsilon^r) * h_E^0(t; d\epsilon^s, R_i), \tag{3.7}$$

where the integral is over all surfaces in E and ρ is the surface reflectivity function. (see Fig. 3.2). The quantities $d\epsilon^r$ and $d\epsilon^s$ represent a differential surface of area dr^2 that is first acting as a receiver from the source S_j and then as a source to the receiver R_i. The surfaces act as receivers with $g(\theta) = cos(\theta) \cdot 1\{\theta < \pi/2\}$ and as first-order Lambertian transmitters.

To estimate $h_E(t; S_j, R_i)$ using (3.7), we consider only M bounces so that

$$h_E(t; S_j, R_i) \approx \sum_{k=0}^{M} h_E^k(t; S_j, R_i). \tag{3.8}$$

The contributions to the overall impulse response from the k-bounce impulse response will decline for increasing k so that excellent approximations can be obtained for M ranging from 3 to 10, as discussed in [15].

3.2.2 Discretization into Facets

The integration in (3.7) is approximated by representing each face F_i at a spatial partitioning factor P , i.e. each face is divided into small elements of size $1/P \times 1/P\ m^2$. Hence we estimate $h_E^k(t; S_j, R_i)$ using

$$h_E^k(t; S_j, R_i) \approx \sum_{n=1}^{N} \rho_{\epsilon_n^r} \cdot h_E^{k-1}(t; S_j, \epsilon_n^r) * h_E^0(t; \epsilon_n^s, R_i), \tag{3.9}$$

where ϵ_n^r and ϵ_n^s represent element n acting as a receiver and source, respectively. The number of elements N is given by

$$N = 2P^2 \sum_{i=1}^{N_b} (L_{x,B_i} L_{y,B_i} + L_{y,B_i} L_{z,B_i} + L_{z,B_i} L_{x,B_i}), \tag{3.10}$$

where B_i is the i^{th} box.

3.2.3 Multi-Receiver Iteration

In (3.9) with $r_i = \epsilon_m^r$ to obtain

$$h_E^k(t; S_j, \epsilon_m^r) \approx \sum_{n=1}^{N} \rho_{\epsilon_n^r} \cdot h_E^{k-1}(t; S_j, \epsilon_n^r) * h_E^0(t; \epsilon_n^s, \epsilon_m^r) = \sum_{n=1}^{N} \alpha_{mn} \cdot h_E^{k-1}(t - \tau_{mn}; S_j, \epsilon_n^r), \tag{3.11}$$

where

$$\alpha_{mn} = V(\overrightarrow{r}_{\epsilon_n^s}, \overrightarrow{r}_{\epsilon_n^r}, E) \frac{\rho_{\epsilon_n^r} T(\Phi_{mn}) g(\theta_{mn})}{P^2 D_{mn}^2} \tag{3.12}$$

and $\tau_{mn} = D_{mn}/c$. The angles Φ_{mn}, θ_{mn} and D_{mn} are the receiver's angle to the source, the source's angle to the receiver and the source-to-receiver distance, respectively, for the source ϵ_n^s , for the receiver ϵ_n^r.

Hence, to calculate $h_E^k(t; S_j, R_i)$, first calculate N impulse responses of $h_E^0(t; S_j, \epsilon_n^r)$. using these, compute $h_E^1(t; S_j, \epsilon_n^r)$ and continued until $h_E^{k-1}(t; S_j, \epsilon_n^r)$ is obtained, at this point it is possible to calculate

$$h_E^k(t; S_j, R_i) \approx \sum_{n=1}^{N} \rho_{\epsilon_n^r} \cdot h_E^{k-1}(t; S_j, \epsilon_n^r) * h_E^0(t; \epsilon_n^s, R_i) \tag{3.13}$$

for each receiver R_i. A key observation is that previously calculated impulse response do not depend on impulse response calculated later, and thus can be computed only once,

independently of the number of receivers involved. Hence, the only calculation required for each receiver is the collection stage given by (3.13). The final calculation stage is to combine the k-bounce impulse responses into an estimate of the overall impulse response, as shown in (3.8).

3.2.4 Multi-Transmitter Iteration

The approach of above section is the most natural and efficient when there are more receiver locations than transmitter locations. The following is an equivalent impulse response calculation when the situation is reversed. i.e. more transmitter locations than receiver locations.

Rewriting (3.7)as

$$h_E^k(t; S_j, R_i) = \int_E \rho_{d\epsilon^r} \cdot h_E^0(t; S_j, d\epsilon^r) * h_E^{k-1}(t; d\epsilon^s, R_i) \tag{3.14}$$

and thus (3.9) as

$$h_E^k(t; S_j, R_i) \approx \sum_{n=1}^{N} \rho_{\epsilon_n^r} \cdot h_E^0(t; S_j, \epsilon_n^r) * h_E^{k-1}(t; \epsilon_n^s, R_i) \tag{3.15}$$

in (3.15) substituting $S_j = \epsilon_m^s$,

$$h_E^k(t; \epsilon_m^s, R_i) \approx \sum_{n=1}^{N} \rho_{\epsilon_n^r} \cdot h_E^0(t; \epsilon_m^s, \epsilon_n^r) * h_E^{k-1}(t; \epsilon_n^s, R_i) = \sum_{n=1}^{N} \alpha_{mn} \cdot h_E^{k-1}(t - \tau_{mn}; \epsilon_n^s, R_i) \tag{3.16}$$

where α_{mn} and τ_{mn} are defined as before.

Hence, to calculate $h_E^k(t; S_j, R_i)$, first calculate N impulse responses of $h_E^0(t; \epsilon_n^r, R_i)$. using these, compute $h_E^1(t; \epsilon_n^r, R_i)$ and continued until $h_E^{k-1}(t; , \epsilon_n^r, R_i)$ is obtained, at this point it is possible to calculate

$$h_E^k(t; S_j, R_i) \approx \sum_{n=1}^{N} \rho_{\epsilon_n^r} \cdot h_E^{k-1}(t; S_j, \epsilon_n^r) * h_E^0(t; \epsilon_n^s, R_i) \tag{3.17}$$

3.3 Implementation And Computational Efficiency

The computation time primarily depends on (a) the maximum number of bounces M, (b) the number of partitions N in the room, and (c) the number of receivers I. From a derivation

given in [22], for a single receiver, the computation time is $O(N^2.M^2)$, while the computation time per receiver T(M,N,I)/I for large I is O(N.M).

For a 5×5 m^2 empty room , and divided into 2400 facets(N). The time Computational time required to calculate a two-bounce impulse response in this scenario for a single receiver is 25 seconds, whereas we can calculate impulse responses for 2500 different receivers (for the same transmitter) in 38 seconds, resulting in a speedup, when compared with the impulse response calculated individually for 2500 receivers, which results in (2500×25) seconds. The calculations were performed on a 1.6 GHz Pentium 4 processor. For very large collections of receivers, the computation time will be dominated by the time to calculate the receiver impulse responses $h_E^k(t; S_j, R_i)$ for each receiver R_i, and not by the time to compute the surface responses $h_E^k(t; S_j, \epsilon_m^r)$. For one-bounce responses, the speedup is much more modest because the most time-consuming operation (calculation of N surface responses from N previous surface responses) is not needed. We are only saved from having to recompute a collection of zero-bounce responses.

3.4 Simulations

Simulation results of infrared channel impulse response are described here.

3.4.1 Simulation Setup

The simulation environment conditions are described here.

1. Room dimensions of $5m \times 5m \times 5m$ are used in the simulation.
2. Reflection coefficients [9] of ceiling and walls are considered as 0.8, where as bottom is considered as 0.3.
3. A Lambertian mode number of 1 is used for the diffusing surfaces.
4. To collect the transmitted impulse response, a $1cm^2$ active area photodetector directed vertically at the ceiling is used.

5. The transmitter is at the center of the room and directed vertically at the ceiling. Total power of transmitted pulse is 1W.

All the calculations in this thesis are two-bounce impulse responses (k=2).

Many assumptions are made for simplicity of calculations.

1. The room is considered as dark room, without any interference, also there are no windows in room to prevent sunlight.

2. There is no loss of power from transmitter to the top(ceiling) of the room. i.e. there is no path loss in this part of transmission.

3.4.2 Design Parameters

A metric to determine the performance of a wireless network is the RMS delay spread, $\Gamma = \sqrt{\overline{\tau^2} - (\overline{\tau})^2}$ [17], where $\overline{\tau} = \sum P(\tau).\tau / \sum P(\tau)$. τ is the delay associated with the signal, relative to the first arriving signal, $P(\tau)$ is the associated power of the signal, $\overline{\tau}$ is the mean delay spread, and $\overline{\tau^2}$ is the second moment of the delay spread. A higher delay spread limits the data rate that can be transmitted, and a conservative estimate of the data rate can be found by calculating the inverse of 10Γ. This data rate does not take into account equalization and other forms of signal conditioning which could be used to increase the data rate.

3.5 Impulse Response Calculations

To analyze the effect of spot patterns and receiver FOV on the system response, the model was run with 4 different spot patterns and 6 different receiver FOVs. Four grid-based designs as shown in Fig.3.3: 2x2, with a 2m separation between the spots; 2x4, with a 1.65m separation; Patterns consisting of a single spot (PT) as well as the case of two spots is considered for simulation. Each pattern had a total of 1W which was equally distributed into all the spots in the design. FOV values of 10^o, 20^o, 30^o, 50^o, 75^o and 90^o were used.

With the detector placed at 2 positions within the room, the received power and delay spread results are tabulated in table 3.1 to table 3.6. At position A, the detector is placed at the exact room center with coordinates (2.5, 2.5, 0.0) and at position B, the detector is placed at the corner of the room with coordinates (0.5, 0.5, 0.0).

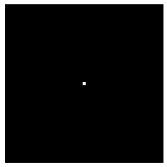

(a) single spot

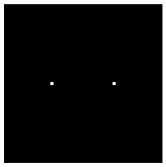

(b) Two spots

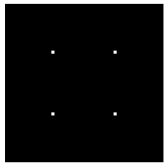

(c) 2×2 Spot Pattern

(d) 2×4 Spot Pattern

Figure 3.3: Spot patterns

The received power is very low for most of the transmitting spot patterns at 10° FOV of the receiver and the placement at the corner, resulting in only 2nd order bounces from the walls to be received by the detector and thus the generally lower receiver power. The

2×2 pattern results in more signal power being received as the wider coverage of the pattern allows some of the 1st order signals from the ceiling to be reflected onto the detector.

However, the tradeoff is that the impulse response is longer compared as to when other patterns are used. When the 10° FOV detector is placed at the room center, the limited FOV only allows 1st order signals from the ceiling to be received. As the 2×2 and 2×4 patterns do not have spots that are within the receiver FOV, no signal is received resulting in a lost connection at the center when these 2 patterns are used. When a single spot lies within the FOV, a negligible delay spread results due to the restriction of multi-paths entering the detector. The greatest amount of power is received when a single spot is used. This is since all the power is concentrated within that single spot and when the single spot falls within the receiver FOV.

Spot Pattern	FOV (deg)	Power Received(μW)		Delay Spread (ns)	
		Pos A	Pos B	Pos A	Pos B
Single	10	0.0866	0.0	0.0	NA
Two	10	0.0086	1.9986e-8	0.1674	0.2498
2×2	10	0.0	7.267e-8	NA	0.2781
2×4	10	0.0	2.399e-7	NA	0.2546

Table 3.1: Metrics from Impulse Response Calculation at 10° FOV

Spot Pattern	FOV (deg)	Power Received (μW)		Delay Spread (ns)	
		Pos A	Pos B	Pos A	Pos B
Single	20	0.1765	2.7450e-6	0.1601	0.2487
Two	20	0.0164	6.6078e-8	0.1696	.2440
2×2	20	0.0140	0.0070	0.17242	0.1724
2×4	20	0.0105	0.0052	0.1723	0.01724

Table 3.2: Metrics from Impulse Response Calculation at 20° FOV

Spot Pattern	FOV (deg)	Power Received (μW)		Delay Spread (ns)	
		Pos A	Pos B	Pos A	Pos B
Single	30	0.227	0.01447	0.1628	0.1834
Two	30	0.01989	0.01291	0.1722	0.1827
2×2	30	0.0197	0.0143	0.1769	0.1828
2×4	30	0.0151	0.0075	0.1755	0.1759

Table 3.3: Metrics from Impulse Response Calculation at 30° FOV

Spot Pattern	FOV (deg)	Power Received (μW)		Delay Spread (ns)	
		Pos A	Pos B	Pos A	Pos B
Single	50	0.227	0.01723	0.1728	0.1853
Two	50	0.02172	0.01651	0.1743	0.1869
2×2	50	0.0202	0.0157	0.1775	0.1851
2×4	50	0.0181	0.01472	0.1811	0.1901

Table 3.4: Metrics from Impulse Response Calculation at 50° FOV

Spot Pattern	FOV (deg)	Power Received (μW)		Delay Spread (ns)	
		Pos A	Pos B	Pos A	Pos B
Single	75	0.227	0.0172	0.1728	0.1853
Two	75	0.02172	0.01651	0.1743	0.1869
2×2	75	0.0202	0.0162	0.1775	0.1863
2×4	75	0.0182	0.0147	0.1811	0.19016

Table 3.5: Metrics from Impulse Response Calculation at 75° FOV

Spot Pattern	FOV (deg)	Power Received (μW)		Delay Spread (ns)	
		Pos A	Pos B	Pos A	Pos B
Single	90	0.227	0.0172	0.17280	0.1853
Two	90	0.02172	0.01651	0.1743	0.1869
2×2	90	0.0202	0.0162	0.1775	0.1866
2×4	90	0.0182	0.0147	0.1811	0.1901

Table 3.6: Metrics from Impulse Response Calculation at 90° FOV

The power received is more as FOV increases, this is due to receiver will detect more multipaths. At 90° FOV it will detect all the signals which fall on the receiver area. However delay spread also increases with increase in FOV.

Chapter 4

OPTIMIZED SIGNAL POWER DISTRIBUTION

4.1 Signal Power Distribution

2500 receivers are placed in the room to calculate signal power distribution and to visualize how the signal power is distributed in the room.

To analyze the results, another metric, the standard deviation of the received power and average delay spread are taken into consideration. From the results, particularly at the narrower FOVs, certain positions may be unable to receive any signals if no sources, either 1^{st} order from the ceiling or 2^{nd} order from the walls, within the receiver FOV. This is particularly prevalent at the corners, which tend to suffer a sharp drop-off in power as compared to positions near the room center. A low standard deviation relative to the average received power would imply that the signal power distribution throughout the receiving plane, in this case the floor, would be more uniform than a high relative standard deviation, and would reduce the drop-off at the corners. Furthermore, a more uniform signal distribution would simplify the design of the receiver electronics by reducing the required dynamic power range of the electronics.

The receiver FOV has a large impact on the system performance. As the FOV is reduced,

the number of multipaths reaching the detector is reduced, which reduces the delay spread, limiting multipath dispersion effects and increasing the possible data rates. However, the tradeoff is that with a reduction in FOV, few paths reaching the detector means that the average received signal power is also reduced accordingly.

At 90°, as earlier mentioned, all signals reaching the detector are accepted. When the FOV is reduced to 45° however, the weaker 2^{nd} order signals from the walls are rejected more than the stronger 1^{st} order signals from the ceiling. For example, when the receiver is placed at the room center, a 45° FOV describes a circle of radius 2.5m at the ceiling. Effectively this means only 1^{st} order signals from the ceiling is accepted. When the FOV is increased to 90° at the same position, the additional power at the receiver is due to the acceptance of 2^{nd} order signals from reflections off the room walls.

FOV(deg)	Average Power(μ_P) μW	Std.Dev of Power (σ_P) μW	Ratio
10	0.09157	0.2866	3.130
20	0.3599	0.4426	1.22968
30	0.7125	0.2459	0.35027
50	0.1601	0.1373	0.18064
75	0.7628	0.13729	0.1799
90	0.763094	0.137322	0.17995

Table 4.1: Signal Power Distribution Parameters for Single Spot

The variation of spot pattern do not have a effect on the performance of the system with a variation of within 10% when different patterns are used. However, the choice of patterns affects the σ_p standard deviation values, with a variation of more than 50% with the standard deviation values, particularly at narrower FOVs. At an FOV value of 10° , σ_p is more than μ_p. A large variation in received power implies that some locations are not receiving any signals. Although an extremely low average delay spread
mu_t is possible at this FOV, alignment is needed for the spot distribution with the room

FOV(deg)	Average Power(μ_P) μW	Std.Dev of Power (σ_P) μW	Ratio
10	0.09157	0.19207	2.0975
20	0.3490	0.3015	0.86414
30	0.6212	0.21195	0.35405
50	0.7268	0.1183	0.1628
75	0.7295	0.11845	0.1623
90	0.7297	0.11848	0.1622

Table 4.2: Signal Power Distribution Parameters for Two Spots

FOV(deg)	Average Power(μ_P) μW	Std.Dev of Power (σ_P) μW	Ratio
10	0.09157	0.1193	1.303
20	0.3380	0.1608	0.4759
30	0.5406	0.20918	0.33862
50	0.6592	0.1004	0.1444
75	0.6978	0.10062	0.1441
90	0.6980	0.10063	0.1440

Table 4.3: Signal Power Distribution Parameters for 2×2 Spot Pattern

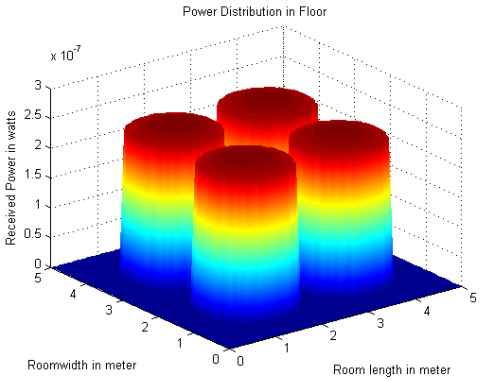

(a) FOV 10°

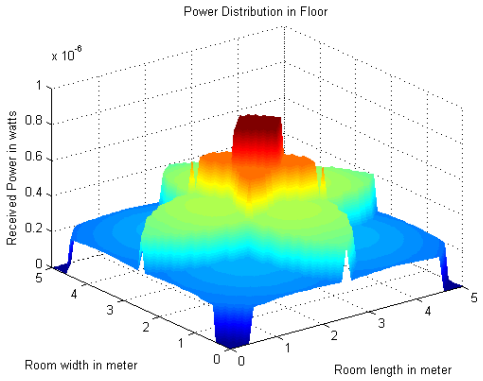

(b) FOV 20°

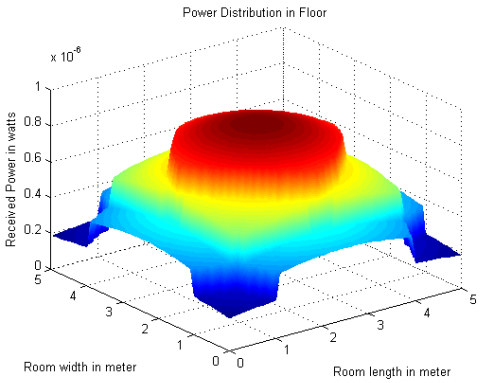

(c) FOV 30°

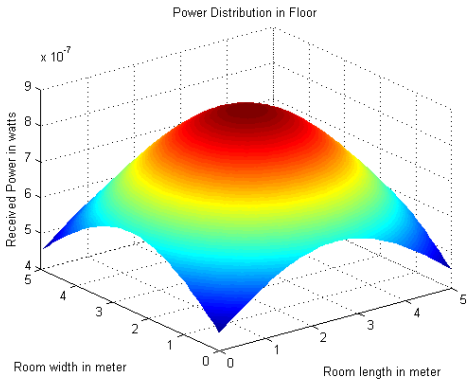

(d) FOV 50°

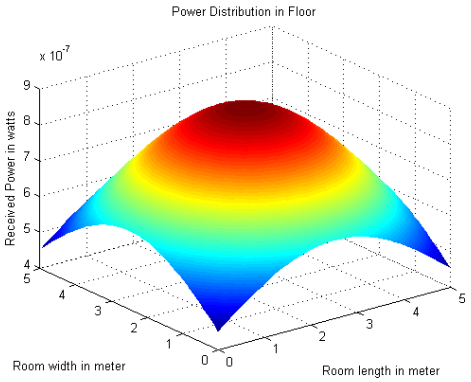

(e) FOV 75°

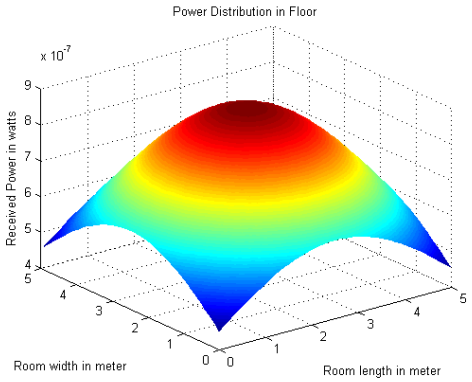

(f) FOV 90°

Figure 4.1: Signal Power Distribution for 2×2 Spot Pattern With Various FOVs

FOV(deg)	Average Power(μ_P) μW	Std.Dev of Power (σ_P) μW)	Ratio
10	0.07040	0.6300	0.8949
20	0.26361	0.9220	0.34977
30	0.4640	0.1362	0.3052
50	0.6279	0.75064	0.11953
75	0.63003	0.7479	0.11871
90	0.6302	0.74806	0.1187

Table 4.4: Signal Power Distribution Parameters for 2×4 Spot Pattern

size to ensure that the receiver is able to receive signals, which may be difficult to ensure practically. The single point and 2×2 spot patterns are clearly unsuitable for use at narrow FOVs as σ_p is larger than μ_p. From Table 4.1, it can be observed that use of a wide FOV of 50° and 90°, allows a low σ_p to be achieved. However, the tradeoff is a higher delay spread due to a larger number of multipaths being allowed to reach the detector. A maximum delay spread of 1.85ns is used as a cutoff value. Using a conservative estimate of $1/(10 \text{ x } \tau)$, this average delay spread value gives a maximum data rate of approximately 54 Mbit/s. Use of equalizers and other communication techniques such as diversity can be used to increase the data rate further but this value is used as a performance benchmark . From the Fig.4.2, the maximum FOV within this benchmark is seen to be 30°.

A larger FOV would also simplify the design of the spot pattern. Using a 20° FOV, for a detector placed at the corner to be able to see a spot, the spot must be less than 2.5m away from the corner. If a 30° FOV detector is used, the spot only need to be less than 6.5m away from the corner, reducing the likelihood of a dropped link if the transmitter is offset from the center. Based on the arguments given above it can be concluded that a receiver FOV of 30° would give a good balance of delay spread and signal power distribution performance.

The performance of the various spot patterns at a 30° FOV is summarized in Fig.4.3. The high standard deviation of the single point and 2×2 spot patterns for received power

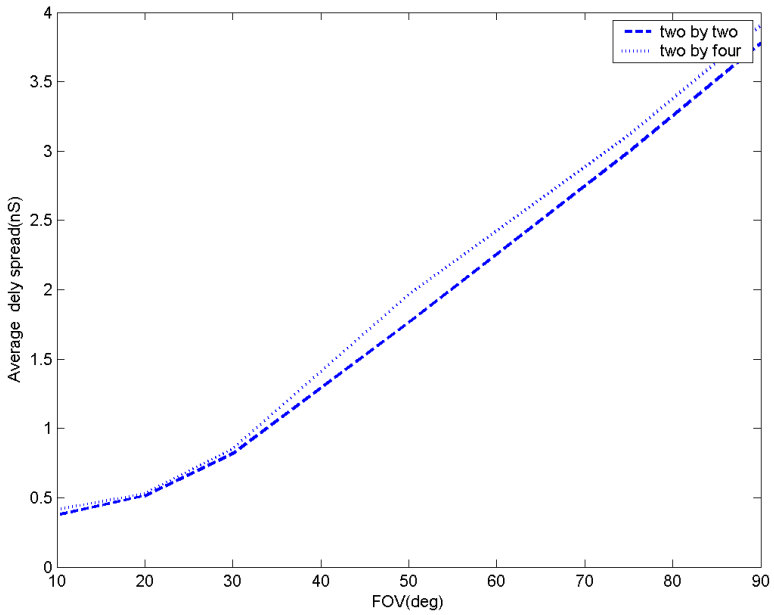

Figure 4.2: Average delay spread as FOV varied with different patterns

indicate a large variation in the system performance, making the pattern clearly unsuitable for use at this FOV value.

The Signal power distribution of various Spot patterns with N = 60,000 at 30° FOV are shown in Fig.4.4. The N value of earlier simulations is 15,000. As the value of N increased , The approximations are more ideal. The values of average received power increases. However, the computational cost also increases. Time taken for calculating signal power distribution with N value 15,000 is 383seconds. With N value 60,000 it is 1593seconds.

On the whole, Ratio doesn't change much. So we used N=15,000 to find optimized spot pattern.

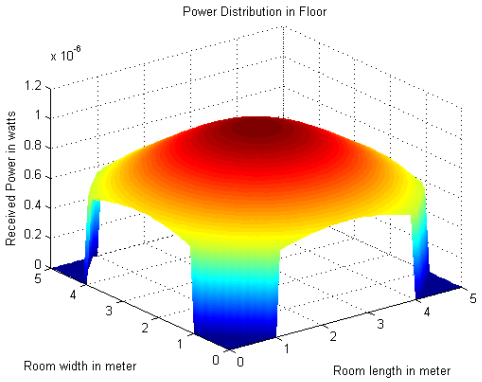

(a) Single Spot

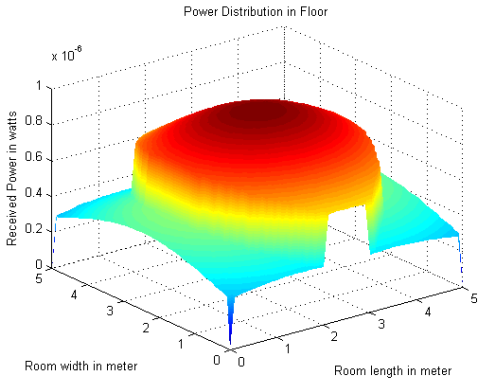

(b) Two Spots

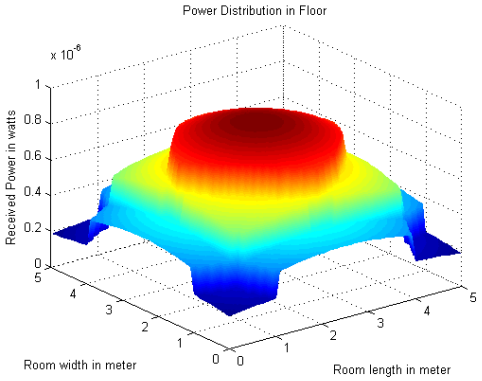

(c) 2×2 Spot Pattern

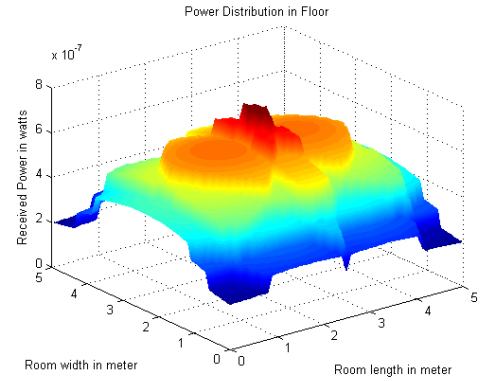

(d) 2×2 Spot Pattern

Figure 4.3: Signal Power Distribution for Various Spot Patterns With FOVs 30°

Spot Pattern	Average Power(μ_P) μW	Std.Dev of Power (σ_P) μW	Ratio
Single Spot	0.72005	0.2429	0.3374
Two Spots	0.62693	0.21843	0.3484
2×2	0.5459	0.20814	0.3812
2×4	0.4498	0.13521	0.3005

Table 4.5: Signal Power Distribution Parameters for various Spot Pattern at 30° FOV

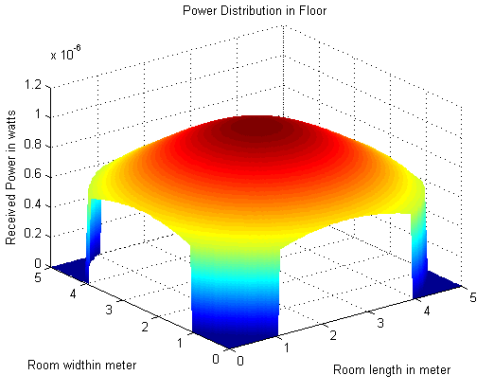

(a) Single Spot

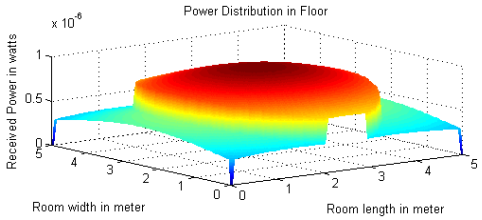

(b) Two Spots

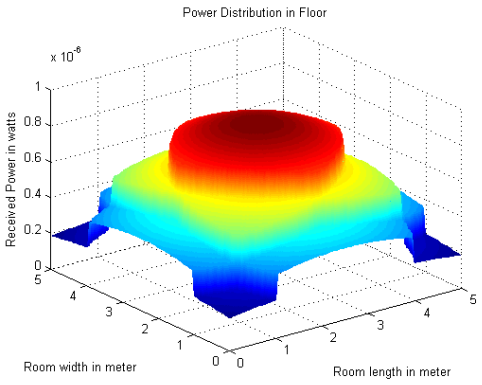

(c) 2×2 Spot Pattern

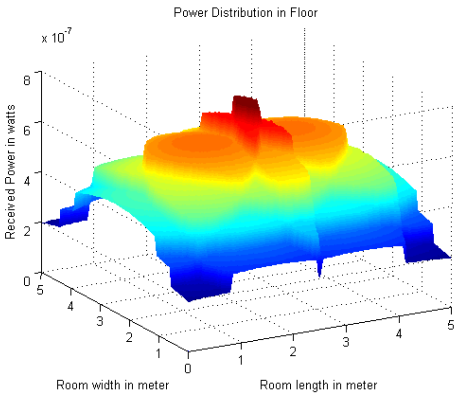

(d) 2×2 Spot Pattern

Figure 4.4: Signal Power Distribution for Various Spot Patterns With FOVs at 30°, N=60,000

4.2 Optimization of Spot Pattern

4.2.1 Simulated Annealing Technique

Using the optimum FOV as determined in above Section , the spot pattern is next optimized using a simulated annealing (SA) technique for this optimum FOV of 30°. The simulated annealing technique was proposed by Kirkpatrick [18] as a means of finding a global minimum in an optimization process. It is analogous to the annealing process of a molten metal, in which a material finds the lowest possible energy state during the cooling process. The chief advantage of using the SA technique is that it avoids being trapped in a local minimum by introducing a temperature coefficient that is slowly reduced. The governing equation is $P = exp(-df/T)$, where P is the probability of accepting an undesired result df, and T is the current temperature. The technique uses a random search process. If a desired result is obtained, the technique accepts the change as the best obtained result. If an undesired result is obtained, that undesired result is accepted with a probability of P. This avoids the algorithm from working on the assumption that the first minimum is the global minimum, as can be the case when a simple iterative minimization (IM) process is utilized, which simply only accepts desirable results with no probability of accepting undesired results. After a number of iterations, T is reduced by a factor of 0.8 [19]. The initial temperature T_0 should result in an average acceptance probability χ_0 of about 0.8 [20], and this can be determined from $-df/ln(\chi_0)$.

In previous work by Yao, Chen and Lim [21], the SA approach was found to be able to optimize the hologram mask to convert a point source into an extended source, with the lowest cost function as compared to the error reduction and input output methods. In this application, the SA algorithm is used to determine the optimum distribution of spots on the room ceiling to achieve a desired performance metric. The algorithm begins with a randomly generated array of spots. A dark pixel represents no illumination by the transmitter, while a light pixel represents a diffusing spot. At each iteration, four pixels which are symmetric about the origin are inverted. If the pixels were previously dark, they are made light, and

if light, are made dark. The relevant metric such as the ratio of standard deviation of the received power to the average received power is calculated, and compared with the previous result to give df, where an undesired result may or may not be accepted depending on P. The iterations are repeated till the end of one cycle, whereby the annealing temperature is reduced, and the cycle of iterations begins for the new temperature. The process can run till either no improvement can be observed or until a set number of cycles have been reached.

In this simulation, initial temperature T_0 is considered as 1, minimum temperature as 1e-8. reduction factor is 0.8. The maximum number of iterations limited to 1600, considering time complexity. Average acceptance probability as $exp(-(df)/(k * T)$.

The simulation started with randomly generated spot pattern. At first, the spots at four corners were inverted and the ratio is been compared with the parent, if it is desired result it will be accepted otherwise it will accepted with probability $exp(-(df)/(k * T)$. This process continued until 1600 iterations, which results in inversion of all spots at least twice. Since top surface (ceiling) is divided into 2500 spots, it will complexly invert all spots nearly 3 times. 1600 iterations are chosen considering time taken for simulation, which is 6 days.

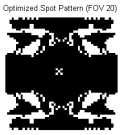

(a) Optimized Spot Pattern

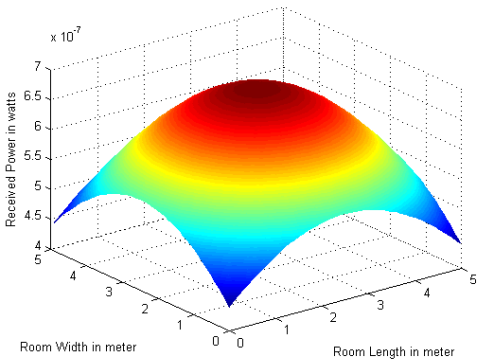

(b) Optimized Field Pattern

Figure 4.5: Optimized Patterns for 20° Fov

Figures 4.5 to 4.9 describes optimized spot patterns at various FOVs and their corre-

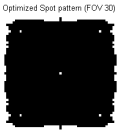

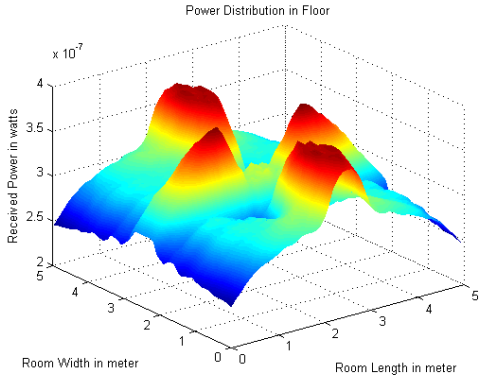

(a) Optimized Spot Pattern (b) Optimized Field Pattern

Figure 4.6: Optimized Patterns for 30° Fov

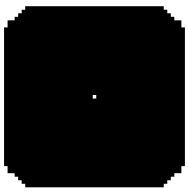

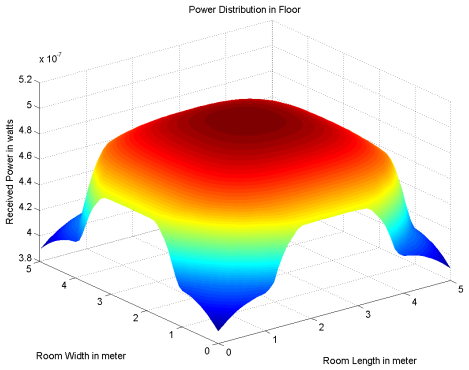

(a) Optimized Spot Pattern (b) Optimized Field Pattern

Figure 4.7: Optimized Patterns for 50° Fov

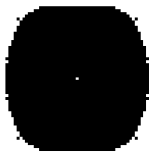

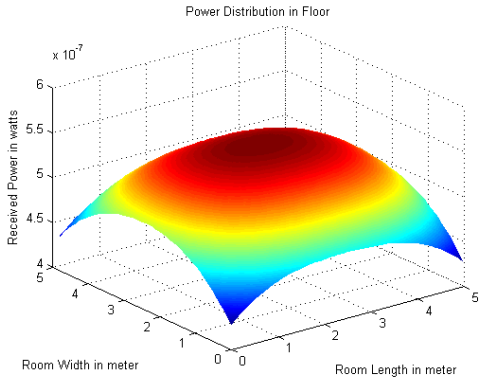

(a) Optimized Spot Pattern (b) Optimized Field Pattern

Figure 4.8: Optimized Patterns for 75° Fov

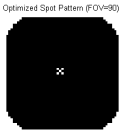

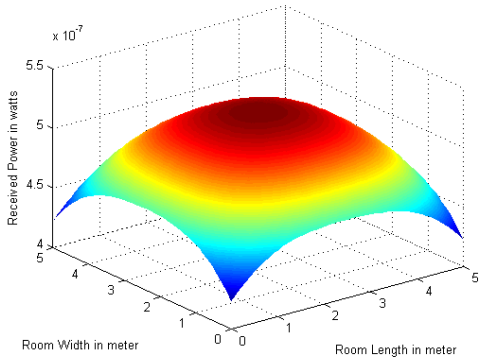

(a) Optimized Spot Pattern (b) Optimized Field Pattern

Figure 4.9: Optimized Patterns for 90° Fov

sponding power distribution in the room. All the optimized patterns are having more white spots at corner rather than at center. The signal power distribution is approximately uniform over receiving surface.

Average received power μ_P and Standard deviation of the average received power σ_P for the optimizing patterns with various FOVs are tabulated. This again shows as FOV increases μ_P increases and σ_P decreases. Hence, the ratio decreases.

FOV(deg)	Average Power(μ_P) μW	Std.Dev of Power (σ_P) μW	Ratio
20	0.59210	0.057006	0.0963
30	0.30207	0.029246	0.0938
50	0.46944	0.027344	0.0582
75	0.50958	0.027253	0.0535
90	0.49026	.022403	0.0457

Table 4.6: Signal Power Distribution Parameters for Optimized Spot Patterns

4.3 Comparison of Results of Conventional Grid Patterns And Optimized Patterns

A comparison is made between the graphs of the conventional grid designs and the optimized results. Using the SA, a reduction of σ_p by a factor of 10 can be achieved. It can be generally observed that this is achieved by having a higher spot density at the edges and corners rather than at the center.

Figure 4.9 shows the comparison of results of optimized spot patterns and conventional grid patterns. Ratio of Standard deviated power to the average received power in the optimized patterns is very less. Though, the ratio graph comes down for some of the higher conventional grid patterns like 4×4, 10×10, delay spread is more. So the technique of using Optimization of spot pattern for a given FOV and specified delay spread(in order to

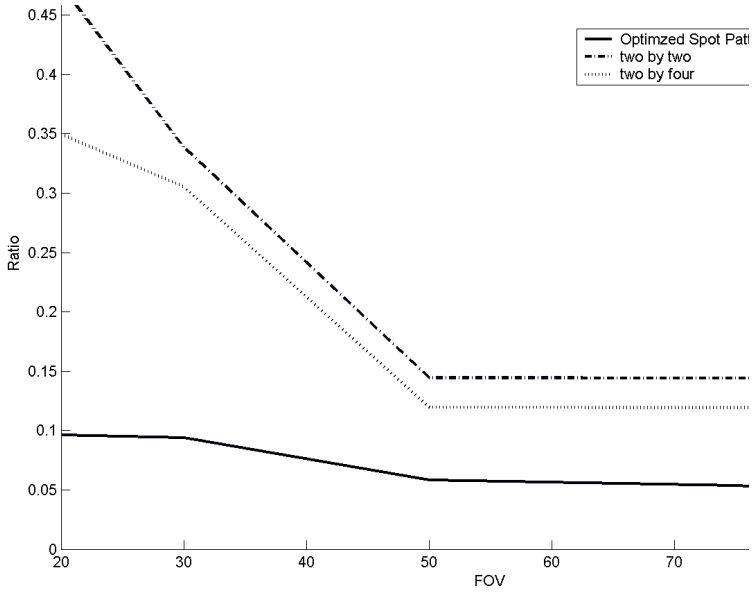

Figure 4.10: Comparison of Results for Optimized Patterns to that of Conventional Grid Patterns

achieve minimum data rate) will give much better performance than any other conventional grid patterns.

Chapter 5

CONCLUSIONS AND FUTURE SCOPE

5.1 Conclusions

The aim of the thesis is to optimize the spot patterns so as to receive uniform power all through the receiving plane. *Multiple Bounce Impulse Response Model* and *Simulated Annealing* technique are used for simulation. conclusions are summarized as follows.

- Impulse response of the indoor optical wireless channel for multiple receivers and multiple transmitters was derived.
- Delay spread of the transmitted optical signal due to multipath propagation is found.
- The effect of FOV on the received signal is observed and compared, FOV value of 30° is found to be the optimum value.
- The effect of spot pattern on the received signal is observed and discussed. If spot pattern is changed all the parameters will change. Positions of spots have more impact than the number of spots.

- The optimized spot pattern at various FOVs, for which, the received power is approximately uniform through out the receiving plane are obtained. SA technique is been is used for this purpose.

5.2 Future Scope

In this thesis, during optimization process delay spread is been used as a constraint. To find the effect of delay spread of the signal we can give weighting factors to the delay spread, and to the ratio of standard deviation of average received power to the average received power. By this, we can get optimized pattern in a much better way, which reduces the ratio much less with specified delay spread.

Computer Generated Hologram (CGH) can be designed [21] to generate particular optimized spot pattern. Once we design CGH, we can simulates whole system and performance can be compared with the existing models of diversity reception.

References

[1] J.M. Kahn and J.R. Barry, "Wireless ifrared communications," *Proc. IEEE*, Feb. 1997, vol. 85, pp. 265-298.

[2] D. Mavrakis: *Measurement and prediction of the wideband indoor radio and infrared channels*, Ph.D. dissertation, University of Surrey, Oct. 2002.

[3] A.C. Boucouvalas, "Indoor ambeint light noise and its effects on wireless optical links," *IEE Proc.: Optoelectronics*, Dec. 1996, vol. 143, pp.334-338.

[4] A.J.C. Moreira, R.T. Valadas, and A.M. De Oliveira Durate, "Performance of infrared trnasmission systems under ambient light interference," *IEE Proc.: Optoelectronics*, vol. 143, Dec. 1996, pp 339-346.

[5] Z. Ghassemloy, "Indoor optical wireless communication systems- Part 1: Review", http://soe.unn.ac.uk/ocr/downloads/part1-rev.pdf,2003.

[6] D.J.T. Heatley, D.R. Wisely, I. Neild, and P. Cochrane, "Optical wireless: The story so far," *IEEE Commun. Mag.*, Dec. 1998, vol. 36, pp. 72-82.

[7] F.R. Gfeller and U.H. Bapst, "Wireless in-house data communication via diffuse infrared radiation," *Proc. IEEE*, Apr. 1993, vol. 67, pp. 1474-1486.

[8] J.R. Barry, J.M. Khan, W.J. Krause, E.A. Lee, and D.G. Messerschmitt, "Simulation of multipath impulse response for wireless optical channels," *IEEE J. Select. Areas Commun.*, Apr. 1993, vol. 11, no.3, pp. 367-379.

[9] J.R. Barry, *Wireless infrared communication*, Boston: Kluwer Academic, 1994.

[10] J.B. Carruthers and J.M. Kahn, " Modelling of non-directed wireless infrared channels," *IEEE Trans. Commun.*, Oct 1997, vol. 45, pp.1260-1268.

[11] V. Jungnickel, T. Haustein, A. Forck and C. von Helmolt, "155Mbit/s wireless transmission with imaging infrared receiver," *Electron. Lett.*, 2001, vol. 37, pp. 314-315.

[12] Infrared Data Association standards can be obtained at the organizations home page on the Web http://irda.org

[13] F. Lopez-Hermandez and M. Betancor, "DUSTIN: algorithm for calculation of impulse response on IR wireless indoor channels," *Electron. Lett.*, Oct. 1997, vol. 33, pp. 1804-1806.

[14] J. M. Kahn, W. J. Krause, and J. B. Carruthers, "Experimental characterization of non-directed indoor infrared channels," *IEEE Trans. Commun.*, February-March-April 1995, vol. 43, no. 2-3-4, pp. 1613-1623.

[15] J. B. Carruthers and P. Kannan, "Iterative site-based modeling for wireless infrared channels," *IEEE Transactions on Antennas and Propagation*, May 2002, vol. 50, pp. 759 -765.

[16] H. Hashemi, G. Yun, M. Kavehrad, F. Behbahani, and P. Galko, "Frequency response measurements of the wireless indoor channel at infrared optics," in *International Zurich Seminar on Digital Communications*, Mar. 1994.

[17] T.S. Rappaport, *Wireless Communications, Principles and Practices*, Prentice-Hall, Upper Saddle River, 2002.

[18] S. Kirkpatrick, C. D. Jr. Gerlatt, and M. P. Vecchi, "Optimization by simulated annealing," *Science*, 1983, vol. 220, pp. 671-680.

[19] S. Kirkpatrick, C. D. Jr. Gerlatt, and M. P. Vecchi, *Optimization by simulated annealing*, IBM Research Report RC 9355, 1982.

[20] S. Kirkpatrick, "Optimization by simulated asnnealing - Quantitative Studies," *J. Stat. Phys*, 1984, vol. 34, pp. 975-986.

[21] J. P. Yao, G. Chen and T. K. Lim, "Holographic diffuser for diffuse infrared wireless home networking," *Opt. Eng*, 2003, vol. 42, pp.317-324.

[22] P. Kannan, *Iterative site-based modeling for wireless infrared channels: an analysis and implementation*, Masters thesis, Boston University, Dept. of Electrical and Computer Engineering, 2001.

[23] J.B. Carruthers and J. M. Kahn, "Angle diversity for nondirected wireless infrared communication," *IEEE Trans. Commun.*, June 2000.

[24] F. J. Lopez-Hernandez, R. Perez-Jimenez, and A. Santamaria, "Ray-tracing algorithms for fast calculation of the channel impulse response on diffuse IR wireless indoor channels," *Opt. Eng.*, 2000, vol. 39, pp. 27752780.

[25] W. A. Arbaugh, "Wireless security is different," *Computer*, 2000, vol. 36, pp. 99-101.

[26] Jeffrey B. Carruthers, Sarah M. Carroll, Prasanna Kannan, " Propagation modeling for indoor optical wireless communications using fast multireceiver channel estimation." *DRAFT*, Oct. 2002.

[27] P. L. Eardley, D. R. Wisely, D. Wood and P. McLee, "Holograms for optical wireless LANs," *Opt. Eng.*, 2002, vol. 41, pp. 899-910.

[28] J. P. Yao, G. Chen and T. K. Lim, "Holographic diffuser for diffuse infrared wireless home networking," *Opt. Eng.*, Feb. 2003, vol. 42, pp. 317-324.

[29] K. Smitha and J.John, " Propagation measurements of indoor infrared channels," *Proc. Photonics-2004*, Dec. 2004.

[30] A.Sivabalan, and J. John, "Modeling and simulation of indoor optical wireless channels," *Proc. IEEE*, TENCON 2003.

[31] Smitha K, *Studies on propagation properties of indoor optical wireless diffuse channels*, Master's thesis, May 2005.

[32] N. Janardhan, *Studies on diffused indoor optical wireless systems*, Master's thesis, Feb. 2001.

[33] Chaturi Singh, J. John, and Y. N. Singh, "Simulation and optimization of the intensity profile of an optical transmitter for high-speed wireless local area networks.", *Proc. Phtonics*, Cochin, Dec. 2004.

[34] Chaturi Singh, J. John, Y. N. Singh, K. K. Tripathi, "Design aspects of high-performance indoor optical wireless transreceivers.", *ICPWC' 2005*, New Delhi, Jan. 2005.